# Two-Photon Initiating Efficiency of a Ditopic Alkoxynitrostilbene Reacting through a Self-Regenerative Mechanism

Nelly Hobeika, Helene Chaumeil, Rana Mhanna, Ming Jin, Xingyu Wu, Arnaud Spangenberg, Davy-Louis Versace, Jean-Pierre Malval

# Two-Photon Initiating Efficiency of a Ditopic Alkoxynitrostilbene Reacting through a Self-Regenerative Mechanism

Nelly Hobeika[1], Helene Chaumeil[2], Rana Mhanna[1], Ming Jin[3], Xingyu Wu[3,1], Arnaud Spangenberg[1], Davy-Louis Versace[4], Jean-Pierre Malval*[1].

[1]*Institute de Science des Matériaux de Mulhouse, UMR CNRS 7361, Université de Haute-Alsace, 15 rue Jean Starcky, Mulhouse, 68057, France*
[2]*Laboratoire d'Innovation Moléculaire et Applications, UMR CNRS 7040, Université de Haute-Alsace, 3 bis rue Alfred Werner, Mulhouse, 68057, France*
[3] *School of Materials Science and Engineering, Tongji University, 4800 Caoan Road, Shanghai, 201804, P.R. China*
[4] *Institut de Chimie et des Matériaux Paris-Est, UMR-CNRS 7182, Equipe Systèmes Polymères Complexes, 94320 Thiais, France*

Correspondance to: Jean-Pierre Malval (e-mail: jean-pierre.malval@uha.fr)

*'Dedicated to the memory of Doctor Olivier Poizat'*

**ABSTRACT.**

The photophysical properties and the photoinitiating reactivity of a ditopic alkoxynitrostilbene were compared to those of its single branch chromophore used as a reference. Whereas a trivial additive effect is observed when considering the one- and two-photon absorption properties, a clear and very significant amplification has been highlighted for the photoreactivity of this free radical photoinitiator which was used as a hydrogen abstractor in presence of an aliphatic amine co-reactant. We indeed demonstrate that the proximity of two nitroaromatics moieties within the same molecular architecture gives rise to an original cycling mechanism based on a stepwise photo triggering of each photoredox center followed by a subsequent regenerative process. The combination of a high two-photon absorption cross-section ($\delta_{780nm} \approx 330$ GM) with a strong enhancement in photoreactivity makes this nitrostilbene bichromophore a very suitable candidate for two-photon polymerization applications.

**Keywords** : Two-Photon Absorption, Nitrostilbenes, Two-Photon Polymerization.

## 1. Introduction.

Two-photon induced polymerization (2PP) has emerged as a strategic technology for the three-dimension patterning of photoactive materials [1, 2]. The 2PP technique consists in tightly focusing of a *fs*-pulse laser beam into a photoactivable resin so as to promote non linear absorption effects which ensure an intrinsic spatial confinement of the phototriggered reaction. The 3D trajectory of the focal point which is translated within the resin medium progressively creates a photopatterned object whose geometry and morphology are initially parameterized using a computer-aided-design (CAD) model. Two-photon initiated polymerization has progressed rapidly as an advanced 3D printing technology which offers a high-quality level writing of complex, 3D structures with feature sizes reaching sub-100 nm scale[3, 4]. The research in 3D nano/microfabrication is highly active owing to its promising applications such as high-density 3D optical data storage[5], biomaterials for regenerative medicine[6], photonic crystals[7], 3D sensors [8, 9] and the like. In the framework of the free radical polymerization, an efficient two-photon initiated reaction implies the use of chromophores which both exhibit a large two-photon absorption cross-section ($\delta$) and an efficient photoreactivity leading to a high yield ($\Phi_i$) for the generation of primary free radicals. Even though the design and development of direct two-photon cleavable initiators appears as a very appealing approach[10, 11], the bicomponent method is, by far, the dominant strategy due to its very simple processability. This method consists in associating two distinctive components in the same acrylate-based formulation: *i)* a two photon active dye whose excited triplet states can promote hydrogen transfer reactions. *ii*) a hydrogen donor co-initiator such as an amine, a thiol or an alcohol which generates the initiating radical. A large set of two-photon absorbing (2PA) systems have been proposed such as fluorone[12], ketocoumarine[13], 4,4'-dialkylaminostilbene[5], or 4,7 diaminofluorene[14]. The main guidelines which motivate the choice of the 2PA chromophore rely on the effective conjugated length within the dye, its electronic symmetry (e.g. dipole, quadrupole) and its dimensionality[15]. The nature and the position of electron donor and acceptor substituents are also of primary importance. Of particular interest, the use of ketones, $\alpha$-diketones or nitro functions[16-18] as acceptor groups can not only promote a strong charge delocalization within the $\pi$-conjugated structure of the dye but can also induce an efficient intersystem crossing yielding a large amount of reactive excited triplet species. In line with this approach, we have previously demonstrated that the *trans*-4-propoxy 4′-nitrostilbene[19] (**PNS** in **Scheme 1**) constitutes a highly reactive 2PA

initiator when associated with an aliphatic amine. For instance, we showed that the two-photon initiating performance of this nitrostilbene was superior by a factor four to that of a 2,7 diaminofluorene derivative used typically for 2PP applications[14, 20, 21]. In the present paper, we extend the analysis to a ditopic alkoxynitrostilbene homologue (**DPNS** in **Scheme 1**). The linear and nonlinear absorption properties as well as the photoinitiating efficiency of **DPNS** have been systematically evaluated and compared to those of its single branch chromophore (**PNS**) used as a reference.

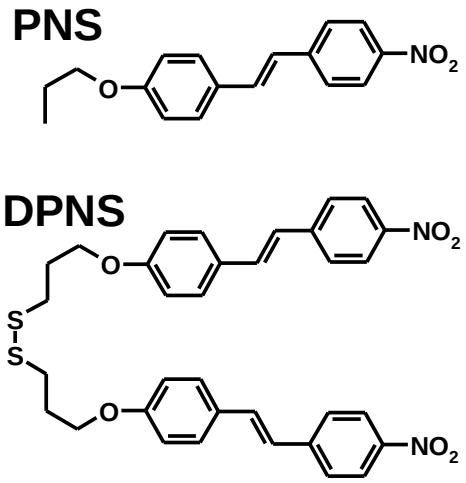


**Scheme 1.** Molecular structures of the nitrostilbene derivatives.

## 2. Results and Discussion

**Ground State Properties. Figure 1** shows the one- (1PA) and two-photon absorption (2PA) spectra of the chromophores in dichloromethane (DCM) along with their respective theoretical absorption spectra calculated at TDDFT-PBE0/6-31G(d,p) level. The corresponding experimental and theoretical data are gathered in **Table 1**. For both compounds the absorption spectrum is dominated by an unstructured band with $\lambda_{MAX}$ of similar values and with an intensity which is twice higher for **DPNS** as compared to **PNS**. The positions of the calculated vertical energy transitions agree very well with the experimental values.

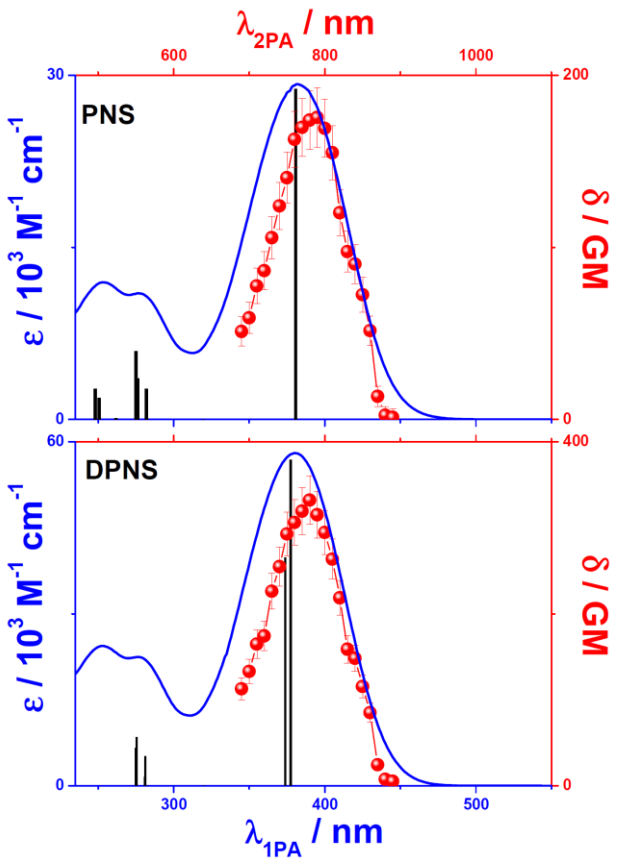


**Figure 1.** Experimental one- (full lines) and two-photon (circles) absorption spectra of **PNS** and **DPNS** in DCM along with their respective theoretical absorption spectra at TDDFT-PBE0/6-31G(d,p) level (vertical bars).

These calculations first indicate that the longest wavelength absorption band of **PNS** can be assigned to the $S_0 \rightarrow S_1$ transition. According to the frontier molecular orbitals diagram depicted in **Figure 2**, this $S_0 \rightarrow S_1$ transition corresponds to a $\pi\pi^*$-type transition with an electronic delocalization along the stilbene fragment and with a clear charge transfer (CT) character from the donor alkoxy group to the acceptor nitro one. By contrast, the TD-DFT

calculations predict that the lowest energy absorption band of **DPNS** encompasses two strongly allowed electronic transitions from the two quasi-degenerate $S_1$ and $S_2$ excited states ($\Delta E_{12}$ ~ 0.02 eV). Both $S_0 \rightarrow S_1$ and $S_0 \rightarrow S_2$ transitions correspond to $\pi\pi^*$-type transitions which are centred on each alkoxynitrostilbene fragment and with the same electronic symmetry as that observed for **PNS** (see **Figure 2**). According to the fully optimized geometry of **DPNS**, it should be underline that the flexible covalent linker between the two ditopic dyes maintains an average distance of ca. 10.5 Å between the oxygen atoms of the alkoxy groups and a distance even larger for the nitro centers (i.e. > 25 Å).

| | ***Experimental*** | | ***Theoretical*** | | | |
|---|---|---|---|---|---|---|
| | $\lambda_{abs}$ / nm | $\varepsilon_{MAX}$ / $M^{-1}cm^{-1}$ | $\lambda_{abs}$ / nm | *f* | Type | Main transitions (fraction) |
| **PNS** | 379 | 29300 | 381 | 0.96 | $\pi\pi^*$ | $H \rightarrow L$ (1) |
| | | | 319 | 0.0002 | $n\pi^*$ | $H_{-4} \rightarrow L$ (0.86) |
| | | | 282 | 0.0021 | $n\pi^*$ | $H_{-4} \rightarrow L$ (0.86) |
| **DPNS** | 377 | 58100 | 377 | 1.23 | $\pi\pi^*$ | $H \rightarrow L_{+1}$ (0.71) / $H_{-1} \rightarrow L$ (0.29) |
| | | | 374 | 0.86 | $\pi\pi^*$ | $H \rightarrow L_{+1}$ (0.29) / $H_{-1} \rightarrow L$ (0.71) |
| | | | 320 | $< 10^{-4}$ | $n\pi^*$ | $H_{-11} \rightarrow L$ (0.84) |
| | | | 319 | 0.0001 | $n\pi^*$ | $H_{-10} \rightarrow L_{+2}$ (0.85) |

**Table 1.** One-photon absorption properties of the chromophores in DCM and their related TD-DFT vertical electronic transitions.

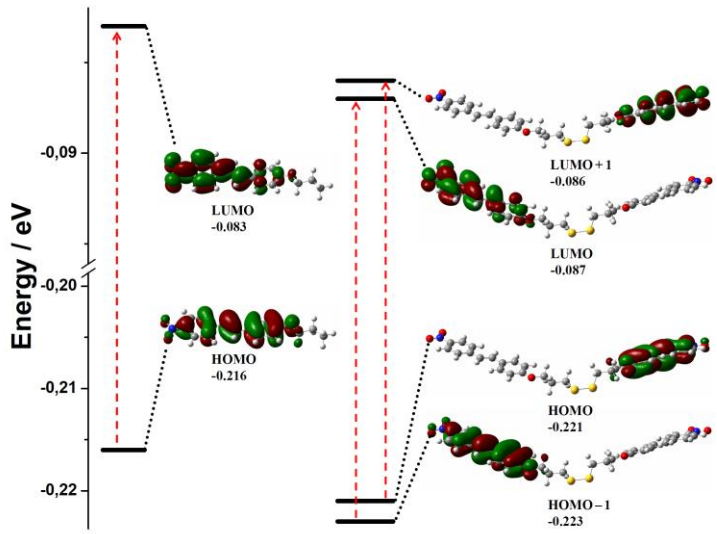


**Figure 2.** Frontier molecular orbital diagrams of the chromophores with the main transitions corresponding to the longest wavelength absorption band.

All these calculations clearly corroborate the fact that the two D-π-A stilbenes even bound together by a saturated chain appear isolated electronically at the ground state. Such an

electronic decoupling can be also illustrated when comparing the redox properties of **DPNS** with respect to those of **PNS**. For instance, **Figure 3** typically shows the cyclic voltammograms (CVs) for the reduction of **PNS** and **DPNS** in dichloromethane. Both CVs exhibit a quasi-reversible reduction wave with redox potentials ($E_{red}$) of similar values (i.e. $E_{red}$ = -1.09 V *vs.* SCE for **PNS** and $E_{red}$ = -1.11 V *vs.* SCE for **DPNS**). These potentials match that of the nitrobenzene[22] which underlines the role of the nitrophenyl subunit as reducible electrophore. Therefore, in the case of **PNS**, the electrochemical reaction should correspond to a one-electron reduction process generating a radical anion (**PNS**$^{\bullet -}$) centred on the nitrophenyl moiety. As shown in **Figure 3**, the reduction of **DPNS** clearly leads to more intensive cathodic and anodic peaks than those measured for **PNS** at the same concentration.

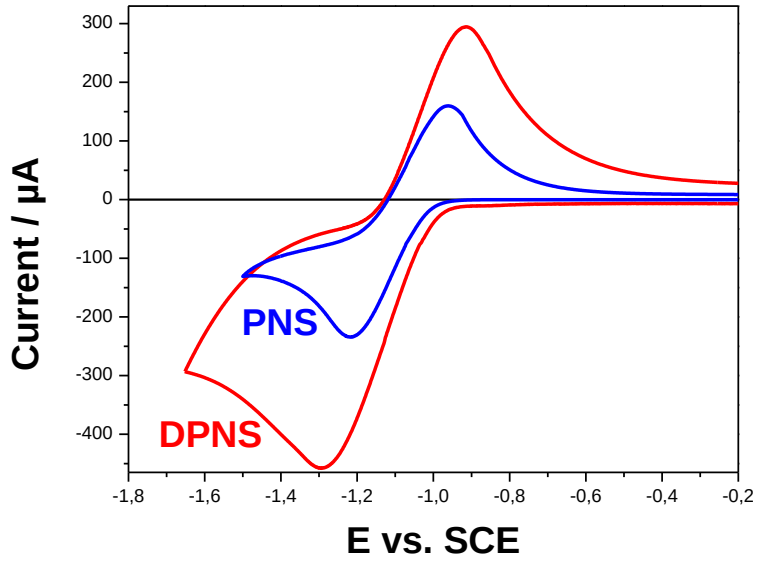


**Figure 3.** Cyclic voltamogramms of **PNS** and **DPNS** in DCM + $(nBu)_4NPF_6$ (0.1 M) on platinum electrode at 200 mV $s^{-1}$ (concentration of chromophores: 2 x$10^{-4}$ M).

This is a clear indication that the two reducible electrophores of **DPNS** are activated at very close redox potentials. Even though one can not assert the occurrence of a two successive one-electron transfers or a single two-electron one[23], this behaviour confirms that the two electrophores are equivalent due to the large distance separating the two nitrophenyl moieties. This large distance should minimise the coulombic repulsion within the electrogenerated di-anion (**DPNS**$^{2-}$) and the subsequent structural changes accompanying the injection of two electrons. Therefore these redox centers can operate independently to each other. This very interesting property will be oriented to trigger sequentially each of these photoredox centers upon two-photon excitation as presented hereafter. The 2PA cross-sections of the dyes have been measured using the two-photon excited fluorescence method[24]. The 2PA spectra of the chromophores are superimposed with their respective 1PA ones in **Figure 1**. According to our

spectral resolution, the two derivatives present a single 2PA band in the 690-880 nm range which reasonably matches their lowest energy 1PA band. The maximum 2PA cross-section ($\delta_{MAX}$) for **PNS** is about 176 ± 13 GM ($\lambda_{MAX}$ ~ 790 nm) in agreement with our previous measurements[19]. Moreover, the superimposition of the 1PA et 2PA spectra confirms that the $S_0 \rightarrow S_1$ transition of **PNS** is two-photon allowed as expected for a $\pi\pi^*$ electronic transition with a strong charge transfer character. In the case of **DPNS**, the additive effect observed for its linear absorption ability as compared to that of **PNS** can be also extended to its 2PA properties. Indeed, the $\delta_{MAX}$ of **DPNS** is about 332 ± 13 GM ($\lambda_{MAX}$ ~ 780 nm) which is roughly twice higher that of **PNS**. This effect is obviously ascribed to the increase in the molecular dimensionality on going from **PNS** to **DPNS**. However, it should be emphasized that $\delta_{MAX}$ increases quadratically with the effective number of π-electrons[25, 26] ($N_{eff}$) contributing to the nonlinear response. A counting method for determining this effective number was proposed by Kuzyk *et al*[25, 26] and consists in calculating $N_{eff}$ by geometrically weighting the number of electrons in each conjugated path of the molecule. The normalization of $\delta_{MAX}$ by $N_{eff}^2$ gives access to the intrinsic 2PA properties of the dyes which allow a better comparison of 2PA performances. According to this methodology, we show that the intrinsic 2PA cross-sections of **PNS** ($\delta_{MAX}$ = 176 GM, $N_{eff}$ = 16) and **DPNS** ($\delta_{MAX}$ = 332 GM, $N_{eff}$ = 22.6) have equivalent values of ca. 0.69 GM and 0.65 GM respectively. Therefore, it is clear that the covalent association of two π-conjugated nitroalkoxystilbenes into a single supramolecular architecture does not lead to a cooperative effect in term of 2PA ability. However, the real advantage of this molecular design strategy will appear when considering the comparative photo reactivity of **DPNS** *vs*. **PNS**.

**Excited State Properties.** The photophysical properties and the relaxation processes associated to the lowest singlet ($S_1$) and triplet ($T_1$) states of **PNS** and **DPNS** have been previously characterized[19, 27]. As illustrated in **Scheme 2**, the locally singlet excited ($^1$LE) of the stilbene derivatives undergoes multiple deactivation processes. First it should emphasized that the addition of a nitro group to an aromatic hydrocarbon[28] is known to 'switch-off' the fluorescence emission properties of the chromophore due to highly efficient competing non radiative channels such as internal conversion (IC) and intersystem crossing (ISC). In this latter case, the presence of $n\pi^*$ states localized on the $-NO_2$ group clearly promotes a very fast ISC process whose rate constant is about ~ $10^{11}$ $s^{-1}$ for **PNS** in apolar medium[29]. However, in our case, **PNS** and **DPNS** still remain fluorescent. Indeed, upon increasing

solvent polarity, the planar $^1$LE state undergoes an adiabatic conformational change corresponding to the rotation of the entire nitrophenyl moiety and generating a highly polar twisted internal charge transfer ($^1$TICT) state[19, 27]. As a typical example, **Figure S1** shows the absorption and fluorescence spectra of both dyes in ethyl ether (low polar solvent) and acetonitrile (highly polar medium). The corresponding spectroscopic data are summarized in **Table S1**. Both nitrostilbenes display very large Stokes shifts which are even more enhanced when increasing polarity. In parallel, the fluorescence quantum yields (see **Table S1**) are amplified by two orders of magnitude on going from ethyl ether to acetonitrile. All these effects clearly evidence a strong electronic and geometrical change between ground and emitting states due to the solvent induced stabilization of this emissive $^1$TICT state. As shown in **Table S1**, the fluorescence 'switch on' of **PNS** and **DPNS** occurrences to the detriment of the *trans*-to-*cis* photoisomerization. This is consistent with the fact that the photoisomerization of the 4,4'alkoxy nitrostilbenes occurs along the $T_1$ surface[29-31] as depicted in **Scheme 2**. Indeed, this reaction implies a barrierless torsion about the olefinic C=C bond generating an intermediate ($^3p$) with a perpendicular configuration. The rapid equilibrium $^3$*trans* ⇆ $^3p$ decays via the ground state of this twisted species into the *trans* or *cis* isomer.

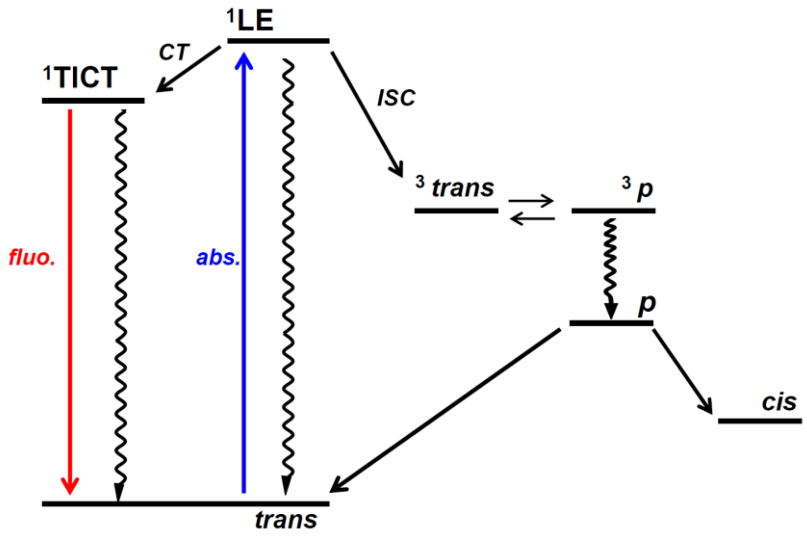


**Scheme 2.** Schematic representation of the multiple deactivation pathways for the excited singlet and triplet states of the nitrostilbene derivatives.

It is noteworthy that **PNS** and **DPNS** exhibit the same excited singlet state energy with a value of ca. $E_{00}$ ~ 2.7 eV in ACN. For **DPNS**, this is a clear indication that the relaxation of the Franck-Condon excited state toward the $^1$LE one implies a localization of the excitation on

a single branch of the molecule. Such an electronic equivalency at singlet state manifold remains true at the triplet state. **Figure 4** shows the luminescence spectra of the chromophores in glassy matrix of 2-methyltetrahydrofuran (2MTHF) at 77 K.

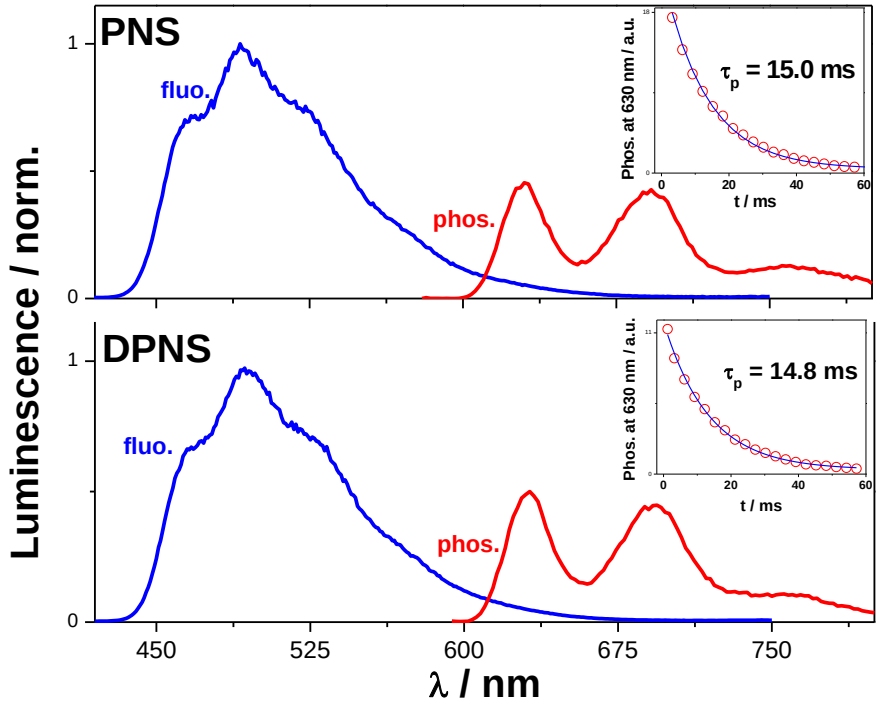


**Figure 4.** Luminescence spectra of **PNS** and **DPNS** in glassy matrix of 2MTHF (77K). Phosphorescence emission was recorded by time-gated method (delay : 1 ms, and time gate : 10 ms)

In glassy matrix, the nitroaromatics derivatives show the same fluorescence and phosphorescence features. The phosphorescence spectrum has a maximum located at 630 nm ($E_T$ ~ 1.97 eV) and clearly presents a vibronic structuration with a progression of three peaks. The triplet phosphorescence lifetime is about ~ 15 ms for both derivatives. All these spectroscopic data confirm that the $T_1$ state of **PNS** and **DPNS** has a $^3n\pi^*$ electronic configuration presumably localized on the $-NO_2$ group. The $n\pi^*$ character of the $T_1$ state undoubtedly constitutes an advantage for promoting hydrogen abstraction reaction in presence of H-donor and initiating thereby free radical photopolymerization of acrylate resins.

**Photoinitiating Ability of DPNS *vs.* PNS and Related Mechanism.** In order to compare the photoinitiating performance of **DPNS** with respect to that of **PNS**, each dye was mixed to a poly(ethylene glycol) diacrylate monomer in presence of N-methyl diethanolamine (**MDEA**). As previously indicated, such an aliphatic amine which is added in a large excess (5 wt %) is

typically used as H-donor reactant. It should be underlined that the concentration of **DPNS** was adjusted to half that of **PNS** in order to obtain isoabsorbing formulations when irradiated at 365 nm (see inset **Figure 5**). The photopolymerization reaction of the laminated acrylate films was monitored by real-time FT-IR and the conversion rates of acrylate double bonds are shown in **Figure 5**.

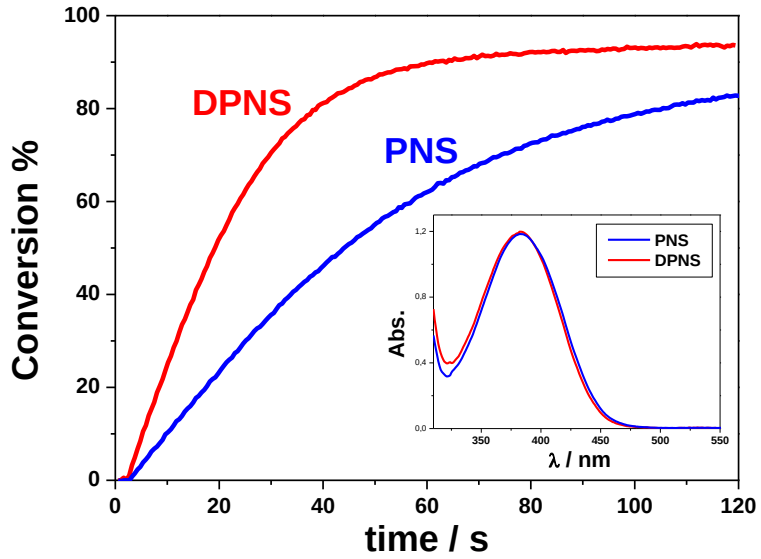


**Figure 5.** Real-time FTIR kinetics of C=C bonds conversion curves upon irradiation of diacrylate formulations ($I_{365nm}$ = 5 mW cm$^{-2}$). Photoinitiating systems: **PNS** / **MDEA** (0.35 wt % / 5 wt %) and **DPNS** / **MDEA** (0.4 wt % / 5 wt %). Inset: Absorption spectra of the corresponding resins (30 µm -thick-films).

The conversion time-profile of **DPNS** formulation clearly presents a much faster dynamics as that observed for **PNS**. For instance, the formulation with **DPNS** reaches 90 % of C=C bonds conversion after 60 s irradiation whereas only 55 % conversion is observed for the **PNS** formulation. The initiation efficiency $\Phi_i$ of these photoinitating systems can be evaluated according to the following equation[32]:

$$\Phi_i = \frac{k_t}{k_p^2}\left(\frac{R_p}{[M]}\right)^2 \frac{1}{I_{abs}} \qquad \text{(eq. 1)}$$

In this equation, $R_p$ corresponds to the rate of polymerization and $I_{abs}$ is the light absorbed by the sample. $k_p$ and $k_t$ are the rate constants for the polymerization propagation and termination steps respectively. Such kinetics parameters are strongly dependent on the structure of the monomer (M). In our precise case, they can be kept constant for both formulations. Based on this formalism, we show that **DPNS** exhibits an initiation efficiency which is 6 times higher than that of **PNS**. In order to explain such a significant amplification in the photoreactivity of

**DPNS**, the photolysis of the nitrostilbenes has been performed in $N_2$-saturated ACN solutions in presence of **MDEA** and methyl methacrylate (**MMA**). **Figure 6** shows the evolution of the absorption spectra of the nitrostilbenes in $N_2$-saturated ACN solutions when irradiated at 365 nm in presence of the distinctive reactants.

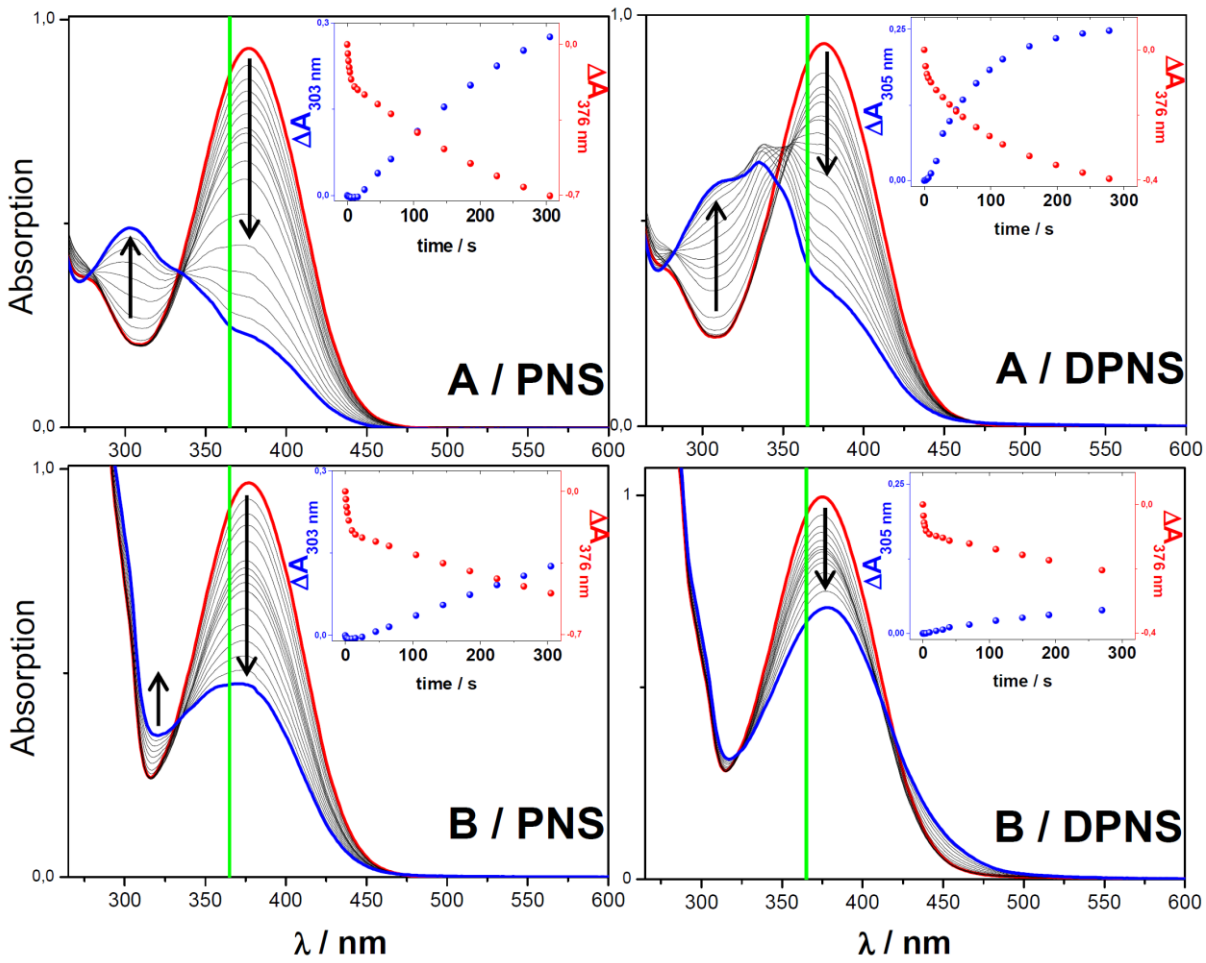


**Figure 6.** Evolution of the absorption spectra of the chromophores in $N_2$-saturated ACN as function of the irradiation time ($\lambda_{irr.}$ = 365 nm, P = 60 mW) : **A / Dye.** Nitrostilbene derivatives mixed with **MDEA** (0.1 M). **B / Dye.** Nitrostilbene derivatives mixed with **MDEA** (0.1 M) and with **MMA** (0.25 M). Vertical lines indicate the spectral position of $\lambda_{irr.}$

First it should be indicated that the photoreaction which induces dyes photobleaching mainly occurs at the triplet state[33, 34] even though the presence amine also leads to a fluorescence quenching of the nitrostilbene chromophores. In this latter case, the Stern-Volmer plots obtained from both steady-state ($I_0/I$) and fluorescence lifetime ($\tau_0/\tau$) measurements show linear correlations as typically illustrated in **Figure S2** for **DPNS** in ACN. The Stern-Volmer constants derived from the slopes of these correlations are slightly higher for **DPNS** as compared to **PNS** with values of ca. 4.4 x$10^9$ $M^{-1}$ $s^{-1}$ and 2.9 x $10^9$ $M^{-1}$ $s^{-1}$ respectively. Note

also that the gradual addition of **MDEA** hardly affects the absorption spectra of the dyes which indicate that the fluorescence quenching of the dyes mainly proceeds through a dynamic process. As shown in **Figure 6A**, the presence of the amine in oxygen-free medium induces a severe decrease of the main absorption band of **PNS** when irradiated at 365 nm. The band decreases concomitantly with the growth of a new one at 303 nm giving rise to several isosbestic points which suggest the occurrence of an equilibrium. In the case of **DPNS**, similar spectral effects can be observed but with the difference that an additional structured band appears in the 325-370 nm range. This new band should be ascribed to the generation of an intermediate by-product. The transient character of this latter species can be highlighted by plotting the absorbance changes at 350 nm as function of the irradiation time as shown in **Figure S3**. According to this absorbance time-profile, the amount of by-product increases until ~ 120 s of irradiation then decreases presumably due to its consecutive consumption. Both for **PNS** and **DPNS**, the global photoreaction progress can be monitored based on the time-dependent profiles of the absorbance at $\lambda_{MAX}$ (376 nm) which mainly reflect the kinetics for the dyes consumption. These kinetics (insets of **Figure 6A**) clearly exhibit two distinctive regimes: *i)* a fast photobleaching step with a half-time of about $\tau_{1/2}$ ~ 3 s for both nitrostilbenes *ii)* a long-time process with $\tau_{1/2}$ of about 245 s for **PNS** and 85 s for **DPNS**. Whereas the first kinetics can be confidently assigned to the fast equilibrium reaction accompanying the *trans*-to-*cis* photoisomerisation process, the second kinetics correspond more specifically to the photoreduction step and the subsequent reactions following this latter process. According to the half-times of this sequence, it is clear that **DPNS** undergoes a faster photobleaching than **PNS**. The photoreduction of the 4-alkoxy 4'-nitrostilbene in presence of aliphatic amine has been thoroughly investigated on the basis of transient absorption and ESR methods[19, 33, 34]. The stepwise photo induced mechanism can be summarized as follows:

$$^3\text{Ar-NO}_2 + \text{MH} \rightarrow \text{Ar-NO}_2^{\bullet -} + \text{MH}^{\bullet +} \quad (1)$$

$$\text{Ar-NO}_2^{\bullet -} + \text{MH}^{\bullet +} \rightarrow \text{Ar-N}^{\bullet}\text{O}_2\text{H} + \text{M}^{\bullet} \quad (2)$$

Upon excitation of the nitrostilbene, an electron transfer is promoted from the amine reactant to the excited triplet state of the dye (step 1). The generated amine radical cation and nitro radical anion can consequently react together through a proton transfer reaction and then produce a nitro H-adduct radical ($\text{Ar-N}^{\bullet}\text{O}_2\text{H}$) and a α-aminoalkyl radical (step 2). This latter radical whose presence has been previously demonstrated by ESR spin trapping methods[19] is

highly reducible[35] and can further reduce a second nitrostilbene dye at the ground state (step 3) as follows:

$$Ar\text{-}NO_2 + M^{\bullet} \rightarrow Ar\text{-}NO_2^{\bullet -} + M^{\bullet +} \quad (3)$$

$$Ar\text{-}NO_2^{\bullet -} + M^{\bullet +} \rightarrow Ar\text{-}N^{\bullet}O_2H + P \quad (4)$$

These two steps also lead to the formation of a second nitro H-adduct radical and other by-products related to the oxidation of $M^{\bullet}$ (step 4). The crucial role of **MDEA** as a sacrificial reactant should be underlined here since it provides two electrons and two protons as depicted in **Scheme S1**. Note that a similar mechanism has been proposed for the photocatalytical reduction of a nitrobenzene series using triethanolamine as reducing agent[36]. The steps (3) and (4) are very interesting since they are globally equivalent to the two previous steps but with the difference that the steps (3) and (4) do not require any excited species. Therefore, according to this global mechanism, two nitro H-adduct radicals are ultimately produced. This species is relatively long living. Indeed, the half-time for the nitro H-adduct radical of the 4-alkoxy 4'-nitrostilbene was estimated in the 1-100 ms range in Ar-saturated ACN[34]. Moreover, it has been demonstrated that these nitro H-adduct radicals undergo an efficient disproportionation [34] yielding a nitroso compound concomitantly with the regeneration of the nitrostilbene dye as follows :

$$Ar\text{-}N^{\bullet}O_2H + Ar\text{-}N^{\bullet}O_2H \rightarrow Ar\text{-}NO + Ar\text{-}NO_2 + H_2O \quad (5)$$

Hence the progressive photobleaching of **PNS** and **DPNS** in presence of **MDEA** should involve successively two nitroaromatics redox centers. The main structural difference between **PNS** and **DPNS** relies on the presence of two nitroaromatics redox centers which are covalently connected together for **DPNS**. Such a structure appears particularly well suited for this multistep mechanism and presents very important advantages: *i)* the cage escape of the α-aminoalkyl radical is not necessary between step (2) and step (3) *ii)* the encountering condition required for the disproportionation in the step (5) is intrinsically fulfilled for **DPNS**. Therefore this mechanism clearly accounts for the ~ 3 times faster photobleaching observed **DPNS** in presence of **MDEA** as compared to **PNS**. As shown in **Figure 6B**, the addition of a methyl acrylate (**MMA**) as third reactant leads to a drastic drop in the production of nitrostilbene by-products whose absorption bands are hardly detected. The presence of **MMA**

clearly opens an alternative reaction route for the consumption of the α-aminoalkyl radical which exhibits a very high reactivity upon addition reactions[37] onto the C=C bonds of the acrylate monomers. These addition reactions certainly compete with the step 3 and should reduce the dyes photobleaching process. This assumption is perfectly in line with the increase of the photobleaching half-time of **PNS** ($\tau_{1/2}$ = 882 s) which is multiplied by a factor 3.6 and that of **DPNS** ($\tau_{1/2}$ = 603 s) whose amplification is even higher with a factor 7.1. Of particular interest, the reduction of the photobleaching rate for **DPNS** is more significant than that observed for **PNS**. This effect suggests that the disproportionation step still remains active for **DPNS**. In this case, the disproportionation of the two nitro H-adduct radicals should mainly proceeds intramolecularly allowing the regeneration of one nitrostilbene branch. By contrast, the disproportionation step appears unlikely for **PNS** due to its diffusion-limited character. For **DPNS**, the occurrence of this regenerative process clearly constitutes an additional source for the further production of α-aminoalkyl radicals and can thereby explain the higher initiation efficiency observed for **DPNS** as compared to **PNS**. We have therefore demonstrated that **DPNS** is a more performant free radical photoinitiator than **PNS** upon one photon excitation. The initiation efficiency ($\Phi_i$) of the bichromophore is about 6 times higher than its reference. Such a significant difference can be extended to two-photon initiated polymerization.

**Two-Photon Polymerization Properties.** The two-photon initiating performances of **PNS** and **DPNS** have been evaluated by two-photon patterning polymer lines using the same diacrylate formulations which were prepared for the one-photon polymerization experiments. The methodology simply consists in focusing a *fs*-pulse laser beam ($\lambda_{exc}$: 780 nm) into the resin using a 40X, 0.65-NA objective. The nonlinear absorption of the nitrostilbenes is then promoted which initiates the polymerization. **Figure 7** typically shows a symmetrical set of polymer lines pattern obtained by the gradual decrease of the laser excitation power for **PNS** and **DPNS** formulations. The progressive decrease of the incident excitation power allows reaching the two-photon polymerization threshold power ($P_{th}$) for each formulation. This fundamental parameter corresponds to the local absorbed-energy density below which the polymerization is not observed (see star pictogram in **Figure 7**). From a mechanistic point of view, this polymerization threshold can be related to the minimum amount of initiating radicals ($[R_0]$) allowing the degree of monomer conversion to past the gelation point.

Therefore $P_{th}$ and $[R_0]$ can be connected by the following equation [1, 38]:

$$[R_0] \propto C.\delta.\Phi_i P_{th}^2 \qquad \text{(eq. 2)}$$

Where C, δ and $\Phi_i$ denote respectively the concentration, the 2PA cross-section and the initiation efficiency of the photoinitiator. As shown in **Figure 7**, the two-photon polymerization thresholds have an estimated power value of 7 mW and 3 mW for **PNS** and **DPNS** formulations, respectively.

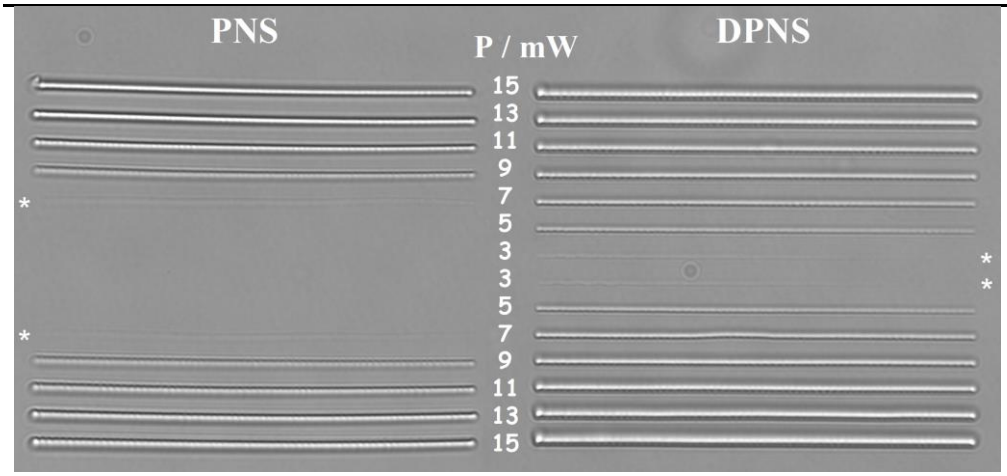


**Figure 7.** Two-photon polymerized lines fabricated for distinctive laser excitation powers ($\lambda_{ex}$ = 780 nm, $\tau_{exp}$ = 2 ms). The star pictogram indicates the corresponding value of $P_{th}$ at 780 nm. Formulations: Poly(ethylene glycol) diacrylate mixed with **MDEA** (wt 5 %) and with : **PNS** (0.35 wt % ↔ 13.6 mM) and **DPNS** (0.4 wt % ↔ 6.8 mM).

Considering that: *i)* the 2PA cross-section of **DPNS** is ~ twice higher that **PNS** *ii)* the concentration of the **DPNS** is half that of **PNS** in this set of formulations. It can be inferred from equation 2 that $(\Phi_i{}^{\mathbf{DPNS}} / \Phi_i{}^{\mathbf{PNS}}) \approx (P^2{}_{th}{}^{\mathbf{PNS}} / P^2{}_{th}{}^{\mathbf{DPNS}})$. According to this methodology, we estimate that the initiating efficiency of **DPNS** is ~ 5.4 higher than that measured for **PNS** which nicely corroborates the comparative photoreactivities of the two nitrostilbenes upon one photon excitation. From a practical point of view, the two-photon initiating performance of a photoinitiator corresponds in fact to the product of its initiation efficiency ($\Phi_i$) with its two-photon absorption ability (δ). In this context, it can be inferred that the two-photon initiation property of **DPNS** clearly outperforms that of **PNS** by about a factor of one order magnitude. Finally, to qualitatively demonstrate the applied potential of **DPNS** as suitable two-photon active initiator, we have inscribed into the **DPNS** diacrylate formulation two arbitrary 2D-microstructures upon excitation at 780 nm (**Figure 8A-B**). In addition, a second

formulation based on pentaerythritol triacrylate (**PETIA**) monomer was prepared with **DPNS** and **MDEA** similarly to the diacrylate formulation. The two-photon polymerization with **PETIA** leads to the formation of a rigid three-dimensional polyacrylate network. Such a macromolecular structuration should guarantee the integrity of photopatterned µ-structures considering the risk of collapse and deformation during the rinsing step of the µ-structure with ethanol. As an illustration, **Figure 8C** shows the scanning electron microscopy (SEM) image of a 2D-grid composed of periodic 20 x 20 µm squares and generated with the **PETIA** formulation. This µ-structure has perfectly resisted to the rising step and displays a good-fidelity replication of the periodic model without any severe deformations.

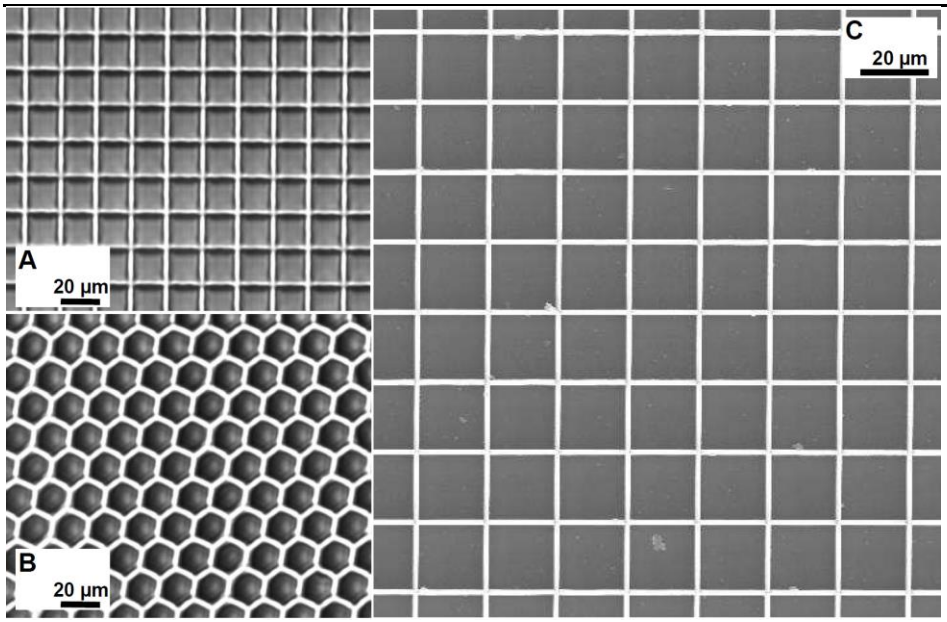


**Figure 8.** **A-B** Transmitted light microscope images of periodic 2D µ-structures. Formulation: diacrylate resin with **DPNS** / **MDEA** (0.4 wt % / 5 wt %). ($\lambda_{ex}$ : 780 nm, P = 5 mW, $\tau_{exp}$ = 2 ms). **C.** SEM images of µ-grid. Formulation: **PETIA** with **DPNS** / **MDEA** (0.4 wt % / 5 wt %). ($\lambda_{ex}$ : 780 nm, P = 5 mW, $\tau_{exp}$ = 2 ms).

## 3. Conclusion.

The one- and two-photon absorption properties of a ditopic alkoxynitrostilbene were compared to those of its single branch chromophore used as a reference. The molecular association of two D-π-A stilbenes with a long saturated linker maintains the electronic integrity of each subunit. An additive effect for the contributions of each single branch to the one and two-photon absorption is observed for the bichromophore which displays a significant 2PA cross-section of about ~ 330 GM at 780 nm. This amplification is much higher when considering the photoreactivity of the bichromophore which can be used as a

H-abstractor in presence an aliphatic amine. The initiation mechanism involves a successive photoactivation of the two nitro centers whose proximity allows a final disproportionation step leading to a regenerative process. By taking advantage of a synergy combining a 2PA additive effect and a strong enhancement in the photoreactivity we show that the two-photon initiation efficiency of **DPNS** is one order of magnitude higher than its reference system.

## 4. Experimental Section.

**Materials.** The synthesis and the characterization of **PNS** and **DPNS** are detailed in reference [19] and [27] respectively. *N*-methyl diethanolamine (**MDEA**) and methyl methacrylate (**MMA**) were purchased from Aldrich. Polyethylene glycol diacrylate monomer (**SR344**) and pentaerythritol triacrylate (**PETIA**) were provided by Sartomer. All the solvents employed were Aldrich spectroscopic grade.

**Steady-state absorption and luminescence spectra.** The absorption measurements were carried out with a Perkin Elmer Lambda 2 spectrometer. Steady-state fluorescence spectra in solution were collected from a FluoroMax-4 spectrofluorometer. Emission spectra are spectrally corrected, and fluorescence quantum yields include the correction due to solvent refractive index and were determined relative to quinine bisulfate in 0.05 molar sulfuric acid ($\Phi$ = 0.52)[39]. The phosphorescence measurements were performed using the same spectrofluorometer which is also equipped with a Xe-pulsed lamp operating at up to 25 Hz. Luminescence measurements were performed in glassy matrix of 2-methyltetrahydrofuran (**2MTHF**) at 77 K. The samples were placed in a 5-mm diameter quartz tube inside a Dewar filled with liquid nitrogen.

**Fluorescence lifetime measurements.** The fluorescence lifetimes were measured using a Nano LED emitting at 372 nm as an excitation source with a nano led controller module, Fluorohub from IBH, operating at 1MHz. The detection was based on an R928P type photomultiplier from Hamamatsu with high sensitivity photon-counting mode. The decays were fitted with the iterative reconvolution method on the basis of the Marquardt/Levenberg algorithm[40]. Such a reconvolution technique allows an overall-time resolution down to 0.2 ns. The quality of the exponential fits was checked using the reduced $\chi^2$ ($\leq$ 1.2).

**Cyclic voltammetry.** The cyclic voltammetry experiments[41] (using a computer-controlled Radiometer Voltalab 6 potentiostat with a three-electrode single compartment cell; the working electrode was a platinum disk; a saturated calomel electrode (SCE) used as a reference was placed in a separate compartment with a salt bridge containing the supporting electrolyte) were performed at 300 K, in $N_2$-saturated dichloromethane with a constant concentration (0.1 M) of n-$Bu_4NPF_6$ ($TBAPF_6$). Ferrocene (Fc) was used as an internal reference.

**DFT calculations.** The theoretical absorption spectra have been computed based on Density Functional Theory (DFT) and Time-Dependent DFT (TDDFT). The overall computation strategy was defined as follows: After initial AM1 optimization calculations (vacuum), subsequent optimization of geometrical structures of the derivatives were carried out using the PBE0/6-31G(d,p) level of calculation. (Note that PBE0 is a good functional for the description of photofunctional molecules[42]). Finally, the TDDFT vertical transitions have been computed using the same level of calculations. All calculations have been performed using GAUSSIAN 09 package[43].

**Photoreactions in liquid medium.** The photoreduction of the nitrostilbene derivatives in presence of coreactants (i.e **MDEA** / **MMA**) was performed in $N_2$-saturated ACN under continuous irradiation at 365 nm with an Hg-Xe lamp (LC 9588/01A from Hamamatsu) equipped with a band pass filter centred at 365 nm (A9616-07 from Hamamatsu). The progress of the reaction was monitored via UV-Vis absorption spectra. The irradiated solutions were continuously stirring and the experiments were performed at 25°C.

**Two-photon excitation fluorescence.** The two-photon absorption (2PA) measurements were performed with femtosecond mode-locked laser pulse using a Ti: Sapphire laser (Coherent, Chameleon Ultra II: pulse duration: ~140 fs; repetition rate: 80 MHz; wavelength range: 680-1040 nm). A relative two-photon excited fluorescence method[24] was employed to measure the two-photon absorption cross-sections, δ. The measurements of 2PA cross-sections were performed relative to reference molecules (*r*) such as fluorescein[24, 44] in water at pH = 11. The value of δ for a sample (*s*) is given by:

$$\delta_S = \frac{S_S \Phi_r \eta_r c_r}{S_r \Phi_S \eta_S c_S} . \delta_r$$

Where $S$ is the detected two-photon excited fluorescence integral area, $c$ the concentration of the chromophores, and $\Phi$ is the fluorescence quantum yield of the chromophores. $\eta$ is the collection efficiency of the experimental set-up and accounts for the wavelength dependence of the detectors and optics as well as the difference in refractive indices between the solvents in which the reference and sample compounds are dissolved. The measurements were conducted in a regime where the fluorescence signal showed a quadratic dependence on the intensity of the excitation beam, as expected for two-photon induced emission. For the calibration of the two-photon absorption spectra, the two-photon excited fluorescence signal of each compound was recorded at the same excitation wavelength as that used for standards (i.e. $\lambda_{exc}$ = 782 nm for fluorescein). The laser intensity was in the range of 0.2-2 x $10^9$ W/cm$^2$. The experimental error on the reported cross section is 15 %.

**Photopolymerization.** The photopolymerization was monitored *in situ* by real-time Fourier transformed infrared spectroscopy with a Thermo-Nicolet 6700 IR-spectrometer. The laminated formulations are sandwiched between two polypropylene films to minimize the inhibiting effect of oxygen. A round teflon spacer is used to maintain a constant thickness of 30 µm. The sample is then positioned between two $BaF_2$ pellets and irradiated using a 100 W Mercury-Xenon Lamp (LC 9588/02A from Hamamatsu) equipped with a band pass filter centred at 365 nm (A9616-07 from Hamamatsu). The conversion rates are obtained from the disappearance of the progressive vinyl C=C stretching vibration band at 1630 cm$^{-1}$.

**Microfabrication.** The 3D lithographic microfabrication was carried out using a Zeiss Axio Observer D1 inverted microscope. The two-photon excitation was performed at 780 nm using respectively a mode-locked Ti: Sapphire oscillator (Coherent, Chameleon Ultra II: pulse duration: ~140 fs; repetition rate: 80 MHz). The incident beam was focused through a 0.65 NA objective (40 X) which leads to a radial spot size 590 nm at $\lambda_{exc}$ = 780 nm (1/e$^2$ Gaussian). A drop of the resin is deposited on a cover slip which is mounted on a 3D piezoelectric stage allowing the translation relative to the laser focal point. The intensity of the entering laser is controlled with the use of an acousto optic modulator. The displacement of the sample and all photonic parameters (i.e. excitation power and irradiation times) are computer-controlled. The

3D microstructure is finally obtained by washing away the unexposed monomer resin using ethanol.

## 5. Acknowledgments

The authors acknowledge the meso-centre ‘EQUIPEX@MESO’ of Strasbourg University for access to High Performance Calculation resources.

## 6. References.


[1] C. N. LaFratta, J. T. Fourkas, T. Baldacchini, R. A. Farrer, *Angew. Chem. Int. ed.* **2007**, *46*, 6238.

[2] K.-S. Lee, R. H. Kim, D.-Y. Yang, S. H. Park, *Prog. Polym. Sci.* **2008**, *33*, 631.

[3] L. Li, R. R. Gattass, E. Gershgoren, H. Hwang, J. T. Fourkas, *Science* **2009**, *324*, 910.

[4] T. F. Scott, B. A. Kowalski, A. C. Sullivan, C. N. Bowman, R. R. McLeod, *Science* **2009**, *324*, 913.

[5] B. H. Cumpston, S. P. Ananthavel, S. Barlow, D. L. Dyer, J. E. Ehrlich, L. L. Erskine, A. A. Heika, S. M. Kuebler, I.-Y. S. Lee, D. McCord-Maughon, J. Qin, H. Röckel, M. Rumi, X.-L. Wu, S. R. Marder, J. W. Perry, *Nature* **1999**, *398*, 51.

[6] J. Torgersen, X.-H. Qin, Z. Li, A. Ovsianikov, R. Liska, J. Stampfl, *Adv. Funct. Mater.* **2013**, *23*, 4542.

[7] T. Ergin, N. Stenger, P. Brenner, J. B. Pendry, M. Wegener, *Science* **2010**, *328*, 337.

[8] L. P. C. Gomez, A. Spangenberg, X.-A. Ton, Y. Fuchs, F. Bokeloh, J.-P. Malval, B. Tse Sum Bui, D. Thuau, C. Ayela, K. Haupt, O. Soppera, *Adv. Mater.* **2016**, *28*, 5931.

[9] S.-Y. Yu, G. Schrodj, K. Mougin, J. Dentzer, J.-P. Malval, H.-W. Zan, O. Soppera, A. Spangenberg, *Adv. Mater.* **2018**, *30*, 1805093.

[10] R. Zhou, J.-P. Malval, M. Jin, A. Spangenberg, H. Pan, D. Wan, F. Morlet-Savary, S. Knopf, *Chem. Comm.* **2019**.

[11] R. Nazir, P. Danilevicius, D. Gray, M. Farsari, D. T. Gryko, *Macromolecules* **2013**, *46*, 7239.

[12] K. D. Belfield, X. Ren, E. W. V. Stryland, D. J. Hagan, V. Dubikovsky, E. J. Miesak, *J. Am. Chem. Soc.* **2000**, *122*, 1217.

[13] R. Nazir, P. Danilevicius, A. I. Ciuciu, M. Chatzinikolaidou, D. Gray, L. Flamigni, M. Farsari, D. T. Gryko, *Chem. Mater.* **2014**, *26*, 3175.

[14] C. Martineau, R. Anémian, C. W. Andraud, I., M. Bouriau, P. L. Baldeck, *Chem.Phys.Lett.* **2002**, *362*, 291.

[15] G. S. He, L.-S. Tan, Q. Zheng, P. N. Prasad, *Chem. Rev.* **2008**, *108*, 1245.

[16] C. Dworak, R. Liska, *J. Polym. Sci. A Polym. Chem.* **2010**, *48*, 5865.

[17] Z. Li, M. Siklos, N. Pucher, K. Cicha, A. Ajami, W. Husinsky, A. Rosspeintner, E. Vauthey, G. Gescheidt, J. Stampfl, R. Liska, *J. Polym. Sci. A Polym. Chem.* **2011**, *49*, 3688.

[18] G. Lemercier, C. Martineau, J.-C. Mulatier, I. Wang, O. Stephan, P. Baldeck, C. Andraud, *New J. Chem.* **2006**, *30*, 1606.

[19] J. P. Malval, F. Morlet-Savary, H. Chaumeil, L. Balan, D. L. Versace, M. Jin, A. Defoin, *J. Phys. Chem. C* **2009**, *113*, 20812.

[20] M. Jin, J. P. Malval, D. L. Versace, F. Morlet-Savary, H. Chaumeil, A. Defoin, X. Allonas, J. P. Fouassier, *Chem. Comm.* **2008**, 6540.

[21] J.-P. Malval, M. Jin, F. Morlet-Savary, H. Chaumeil, A. Defoin, O. Soppera, T. Scheul, M. Bouriau, P. L. Baldeck, *Chem. Mater.* **2011**, *23*, 3411.

[22] N. Leventis, A. Dass, *J. Am. Chem. Soc.* **2005**, *127*, 4988.

[23] D. H. Evans, *Chem. Rev.* **2008**, *108*, 2113.

[24] C. Xu, W. W. Webb, *J. Opt. Soc. Am. B* **1996**, *13*, 481.

[25] M. G. Kuzyk, *J. Chem. Phys.* **2003**, *119*, 8327.

[26] J. P. Moreno, M. G. Kuzyk, *J. Chem. Phys.* **2005**, *123*, 194101.

[27] N. Hobeika, J.-P. Malval, H. Chaumeil, V. Roucoules, F. Morlet-Savary, D. L. Nouen, F. Gritti, *J. Phys. Chem. A* **2012**, *116*, 10328.

[28] O. F. Mohammed, E. Vauthey, *J. Phys. Chem. A* **2008**, *112*, 3823.

[29] G. Gurzadyan, H. Görner, *Chem. Phys. Lett.* **2000**, *319*, 164.
[30] H. Görner, D. Schulte-Frohlinde, *J. Phys. Chem.* **1978**, *82*, 2653.
[31] H. Görner, D. Schulte-Frohlinde, *J. Photochem.* **1978**, *8*, 91.
[32] J. P. Fouassier, *Photoinitiator, Photopolymerization and Photocuring: Fundamentals and Applications*, Hanser, New York, **1995**.
[33] H. Görner, D. Schulte-Frohlinde, *Chem. Phys. Lett.* **1986**, *124*, 321.
[34] H. Görner, *Phys. Chem. Chem. Phys.* **2002**, *4*, 482.
[35] D. D. M. Wayner, D. Griller, *J. Am. Chem. Soc.* **1985**, *107*, 7764.
[36] X.-J. Yang, B. Chen, L.-Q. Zheng, L.-Z. Wu, C.-H. Tung, *Green Chem.* **2014**, *16*, 1082.
[37] S. C. Ligon, B. Husar, H. Wutzel, R. Holman, R. Liska, *Chem. Rev.* **2014**, *114*, 557.
[38] T. Baldacchini, C. N. LaFratta, R. A. Farrer, M. C. Teich, B. E. A. Saleh, M. J. Naughton, J. T. Fourkas, *J. Appl. Phys.* **2004**, *95*, 6072.
[39] R. Meech, D. Phillips, *J. Photochem.* **1983**, *23*, 193.
[40] D. V. Connor, D. Phillips, *Time correlated single photon counting* , Academic Press, London, **1984**.
[41] J. P. Malval, C. Chaimbault, B. Fischer, J. P. Morand, R. Lapouyade, *Res. Chem. Interm.* **2001**, *27*, 21.
[42] S. Aloïse, Z. Pawlowska, C. Ruckebusch, M. Sliwa, J. Dubois, O. Poizat, G. Buntinx, A. Perrier, F. Maurel, P. Jacques, J.-P. Malval, L. Poisson, G. Piani, J. Abe, *Phys. Chem. Chem. Phys.* **2012**, *14*, 1945.
[43] M. J. Frisch, in *Gaussian 09, Revision B.01, Gaussian, Inc., Wallingford CT*, Wallingford CT, **2009**.
[44] M. A. Albota, C. Xu, W. W. Webb, *Appl. Opt.* **1998**, *37*, 7352.

## Table of Contents

A two-photon activable ditopic alkoxynitrostilbene was developed to promote free radical photoinitiation reactions. Taking benefit of a synergy between high two-photon absorption cross-sections ($\delta_{780\ nm}$ ~ 330 GM) and a regenerative photoinitiation process, the bichromophore clearly exhibits an amplified two-photon induced reactivity and constitutes a promising candidate for two-photon polymerization applications.